



Study of theoretical uncertainties in Z and $Q\bar{Q}$ cross sections and the sensitivity to pdf and α_s determination from Z and $Q\bar{Q}$ measurements.

Bodo Schwabe, University of Goettingen, Germany

September 4, 2013

Abstract

During the summer student programm 2013 I investigated various uncertainties within the Z , $t\bar{t}$ and $b\bar{b}$ production cross sections. First, I selected the subprocesses contributing to the overall production cross sections and also analysed them depending on the rapidity y and the transverse momentum p_T . In a second step, I focused on the different uncertainties yielding the overall uncertainties on the production cross sections. Finally, I compared the production cross sections as predicted by different PDFs.

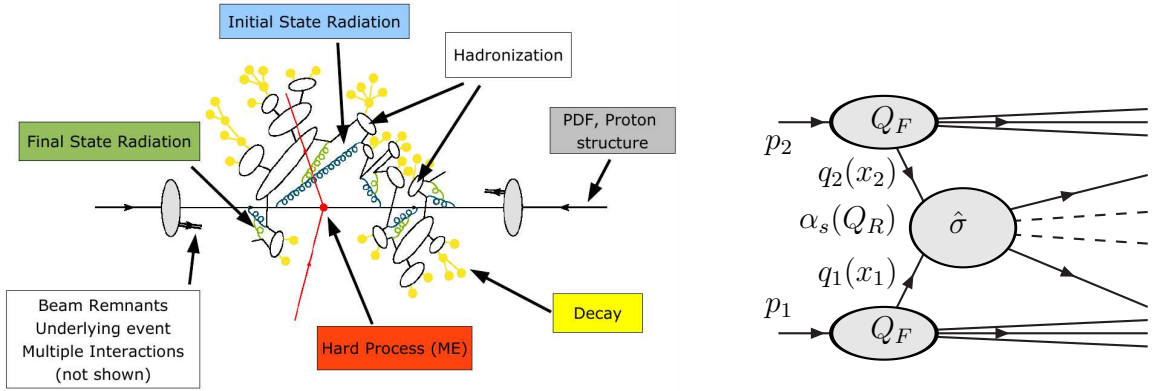
Contents

1	The factorization theorem	3
2	Event generation	4
3	Analysing production channels	5
4	Analysing cross section uncertainties	7
5	Comparing PDFs	8
6	Conclusion	11

1 The factorization theorem

Scattering events as they occur, e.g. within the ATLAS detector at CERN, are rather complex as one can see in figure 1(a). Though, the factorization theorem [1] can be used to calculate cross sections. It uses the fact, that the various subprocesses leading to the overall scattering event take place at very different time scales and therefore can be factorized. Since the hard production process takes place at very short time scales the partons of the protons can be assumed to be at rest. Then, looking only at the differential production cross section with respect to some observable X (fig. 1(b)), it reads:

$$\frac{d\sigma}{dX} \sim \sum_{(i,j,p)} \int d\Gamma \alpha_s^p(Q_R^2) q_i(x_1, Q_F^2) q_j(x_2, Q_F^2) \frac{d\hat{\sigma}_{(p)}^{ij}}{dX}(x_1, x_2, Q_F^2, Q_R^2; S) . \quad (1)$$



(a) sketch of a scattering event with all its different subprocesses taking place at very different time scales

(b) sketch to explain the factorization of a production cross section as described by eq. 1

Figure 1: Illustration of the factorization theorem

Here $\alpha_s^p(Q_R^2)$ is the running coupling constant depending on the renormalization scale Q_R^2 , the parton density functions (PDF) give the probabilities to find a parton $q_i(x_1, Q_F^2)$ with momentum x_1 and a parton $q_j(x_2, Q_F^2)$ with momentum x_2 at the factorization scale Q_F^2 . These factors are non-perturbative inputs that have to be extracted from data. They factorize from the hard scattering process $\frac{d\hat{\sigma}_{(p)}^{ij}}{dX}(x_1, x_2, Q_F^2, Q_R^2; S)$, which also depends on the center of mass energy S . This factor is calculable perturbatively from Feynman diagrams. In order to get the differential cross section the integral has to be summed over the various flavours i, j and the different orders p of the perturbation series. In this analysis the following PDFs are investigated:

- cteq66
- CT10nlo

- NNPDF21-100
- NNPDF23-nlo-as-0119
- NNPDF23-nlo-noLHC-as-0118
- MSTW2008nlo90cl
- HERAPDF15NLO-EIG
- GJR08VFnloE
- abm11-5n-nlo

2 Event generation

In order to produce the cross section predictions that are analysed in the following, the program LHAPDF (Les Houches Accord PDF Interface [2]) was used. It provides a unified and easy to use interface to the PDF sets listed above. They were then evolved by HOPPET (Higher Order Perturbative Parton Evolution Toolkit [3]), a Fortran 95 package for carrying out QCD DGLAP evolution and other common manipulations of PDFs. For the calculation of the matrix elements and the resulting cross-sections the program MCFM (Monte Carlo for FeMtobarn processes [4]) was used, which is designed to calculate cross-sections for various femtobarn-level processes at hadron-hadron colliders. For most processes, matrix elements are included at next-to-leading order and incorporate full spin correlations.

As these calculations would be too time consuming, with calculations of NLO cross-sections taking days, during the whole analysis the program APPLgrid [5] was used in addition. It relies on the factorization theorem described in the last section as it splits the calculation into two parts by storing the weights from the Monte Carlo sampling of the phase space in a grid and then performs the convolution externally ¹. In this way fast convolutions of the (N)NLO weights with any given PDF and variations of renormalisation and factorisation scales are possible.

More explicitly, the matrix elements are presented as a sum over $m = 1, \dots, N$ weights, ω_m , from Monte Carlo integration:

$$d\sigma = \sum_p \sum_{m=1}^N \omega_m^{(p)} \left(\frac{\alpha_s(Q_m^2)}{2\pi} \right)^p q_1(x_{1m}, Q_m^2) q_2(x_{2m}, Q_m^2) .$$

It is important to note that there is an implicit summation over parton flavours. It is therefore helpful to make use of symmetries in the matrix elements to use a vector,

¹Explanations taken from <http://indico.cern.ch/getFile.py/access?contribId=185&sessionId=4&resId=0&materialId=slides&confId=86184> on 2013-09-02 at 11:16

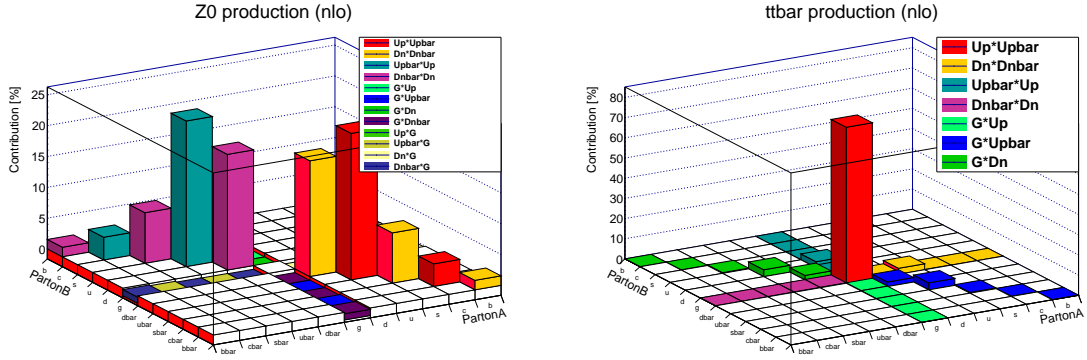
$k = 1, \dots, M$ of indendent weights such that:

$$\sum_{ij=q,\bar{q},g} \omega_{ij} q_{1i}(x_1) q_{2i}(x_2) = \sum_{k=1}^M \omega^{(k)} F^{(k)}(x_1, x_2) .$$

For the production processes investigated here this is graphically shown in fig.2. Now, the cross section can be written as

$$d\sigma = \sum_p \sum_{k=1}^M \sum_{m=1}^N \omega_m^{(p)(k)} \left(\frac{\alpha_s(Q_m^2)}{2\pi} \right)^p F_m^{(k)}(x_{1m}, x_{2m}, Q_m^2) ,$$

which can be placed on a grid. Then, n^{th} order Lagrange interpolation can be used to replace the summation over events by summation over grid points. After the grid generation the cross section can be calculated separately at each order. In this way various cross sections can be efficiently calculated using different PDFs, beam energies, renormalisation and factorisation scales.



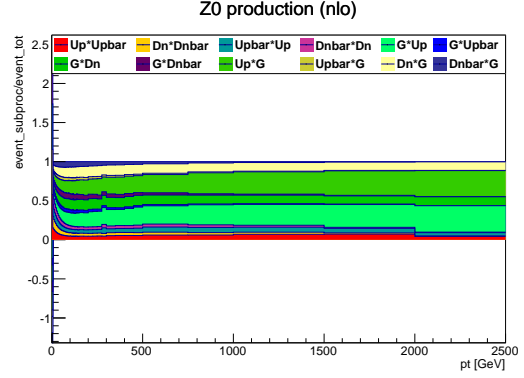
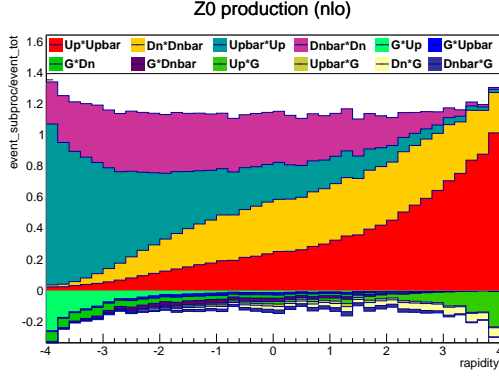
(a) Illustration of the NLO subprocesses contributing to the Z production cross section. Neglecting masses it can be seen that out of the 11x11 channels only 12 independent channels contribute.

(b) Illustration of the NLO subprocesses contributing to the TTbar production cross section. Neglecting masses it can be seen that out of the 11x11 channels only 7 independent channels contribute. The contributing channels to the BBbar production cross section are the same and are also highly dominated by gluon fusion.

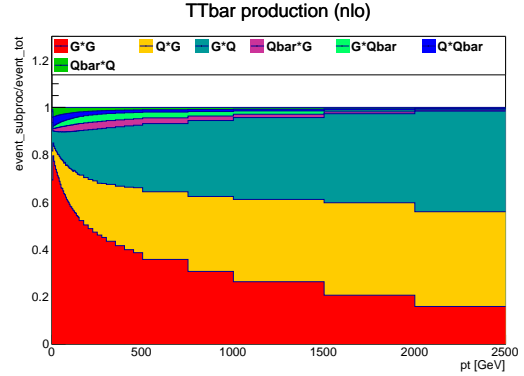
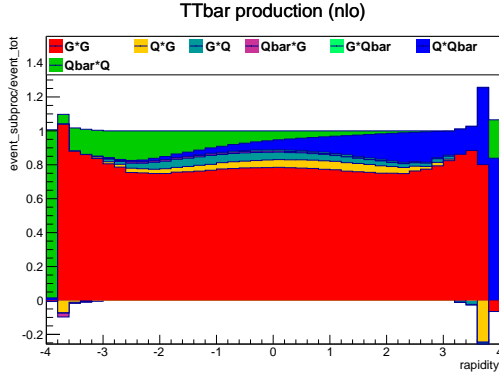
Figure 2: Identifying channels contributing to the production cross section

3 Analysing production channels

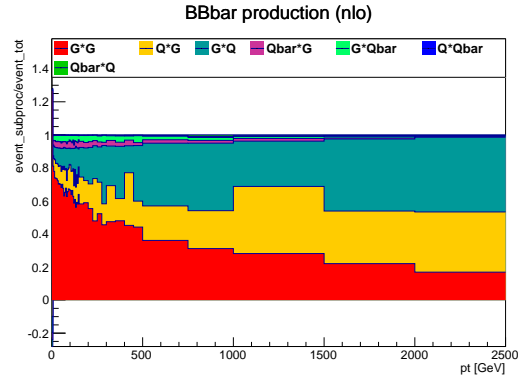
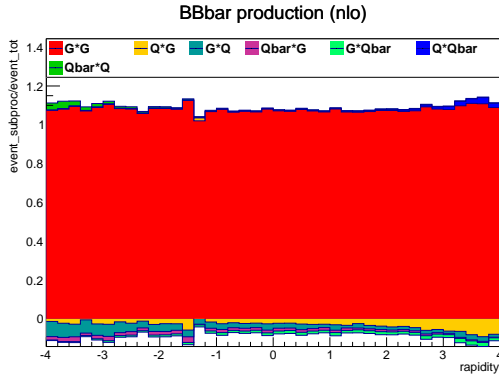
During my 2013 summer school project I investigated Z , $t\bar{t}$ and $b\bar{b}$ production cross sections. In fig.2 the relevant subprocesses were already shown, but only with respect to their overall contribution to the production cross section. Depending on the rapidity y and the transverse momentum p_T their contributions are shown in fig.3.



(a) Z production is dominated by quark pair fusion channels involving gluons are only p_T . That's why the production is dominated by NLO corrections. It can be seen that they contribute destructively, as their contributions are negative. The process is almost symmetric with respect to the sign of y .



(c) The $t\bar{t}$ production is highly dominated by gluon fusion and is symmetric with respect to the sign of y . The peaks on each side are unphysical in the low p_T range. For higher p_T quark gluon fusion channels are much more important.



(e) $b\bar{b}$ pairs are almost exclusively produced by gluon fusion. The process is again symmetric with respect to the sign of y .

(f) As for the $t\bar{t}$ production the dominance of the gluon fusion channel is due to its dominance in the low p_T range. For higher p_T quark gluon channels are much more important.

Figure 3: Channels contributing to the production cross sections depending on the rapidity y and the transverse momentum p_T

It was found that the production channels are very symmetric with respect to the sign of y . While the Z boson is mainly produced via quark pair annihilation, the quark pair production is dominated by gluon fusion. Looking at the contributions depending on p_T this dominance is a low p_T phenomenon as most events accure in the low p_T region. For large p_T different channels become important.

4 Analysing cross section uncertainties

Next I investigated the different contributions to the overall cross section uncertainties of the Z , $t\bar{t}$ and $b\bar{b}$ production. Exemplary, the results are graphically shown in fig.4-6 for the PDF 'CT10nlo' only. Though, the analysis has been done for all the PDFs mentioned above. The considered contributions were always:

- The renormalization and factorization scales (R+F scales) where the uncertainties shown were produced by multiplying both scales by a factor of two or one half to get the upper or lower bound respectively.
- The PDF uncertainties that were provided with the PDFs.
- The uncertainty of the strong coupling constant α_s .

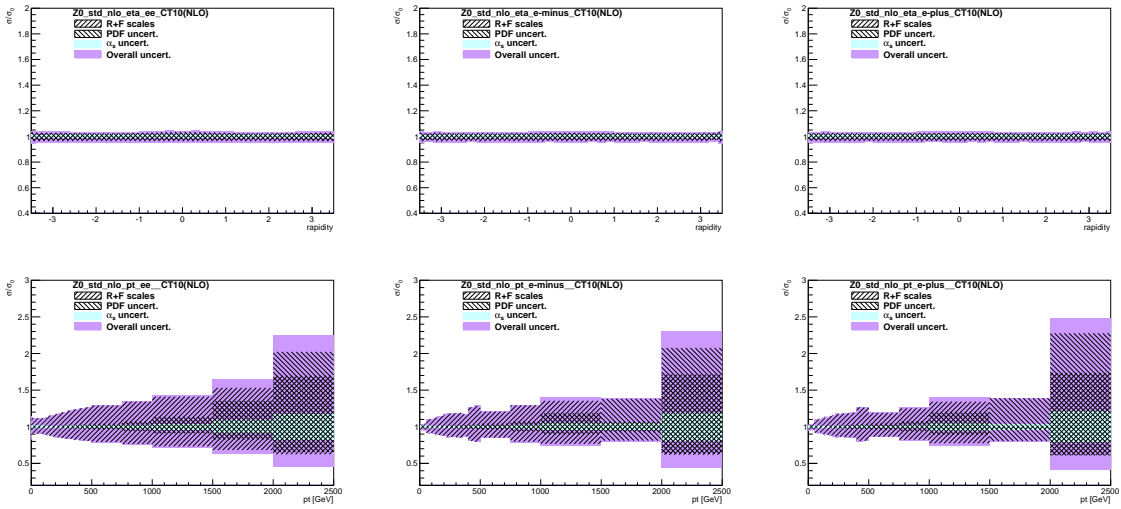


Figure 4: Uncertainties in Z production. From left to right the plots are shown for the lepton pair, lepton and antilepton in the final state. The cross sections σ normalized to the reference cross section without error bands σ_0 are shown with respect to y (first row) and p_T (second row).

The resulting cross sections σ were always plotted against the reference cross section without any errors σ_0 . Thus, the error bands around the constant line at one. In fig.4 and

5 it can be seen that the Z and $b\bar{b}$ production cross sections do not depend on the rapidity and have a narrow uncertainty band of 5% for Z and 20% for $b\bar{b}$ production. Though, the uncertainties are increasing with higher transverse momentum. Especially large contributions come from the R+F scale uncertainties, which implies the need of higher order cross section calculations as these uncertainties can only be improved that way. For very high p_T the PDF uncertainties steeply rise as well, as their parametrisations don't fit well in this region anymore. Qualitatively the same picture is seen when looking at the leptons/quarks separately.

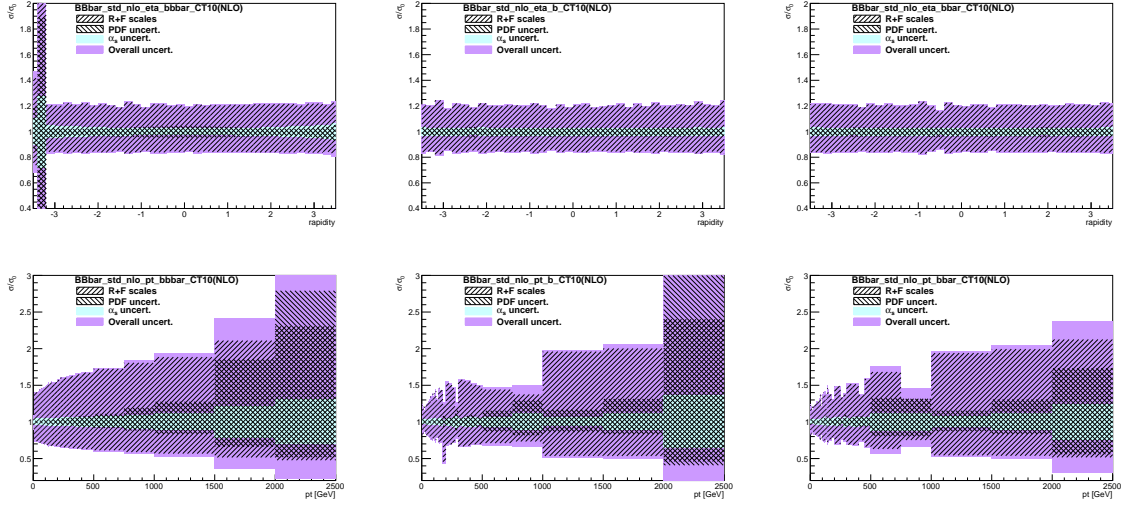


Figure 5: Uncertainties in $b\bar{b}$ production. From left to right the plots are shown for the $b\bar{b}$ pair, b and \bar{b} in the final state. The cross sections σ normalized to the reference cross section without error bands σ_0 are shown with respect to y (first row) and p_T (second row). The peak on the left of the first plot is unphysical and due to insufficient amounts of events generated in this region.

The top pair production is rather different (fig.6). Here the uncertainties strongly increase with higher $|y|$ mainly due to PDF uncertainties. In this regime the PDFs parametrisation seems to be not valid anymore. The same picture is seen when looking at the single tops. The rise of the uncertainties with respect to higher transverse momentum is comparable to the one seen in the Z and $b\bar{b}$ production when focusing on the top pair. Unfortunately, the behaviour for the single tops and antitops does not look very consistent. This is most likely due to some error during the event generation. Here new data should be taken and be compared to the existing analysis. Though, this will be left for further studies.

5 Comparing PDFs

In the last part of my research project I compared production cross sections as predicted by different PDF's. Again I will only use 'CT10nlo' as a reference, though the analysis

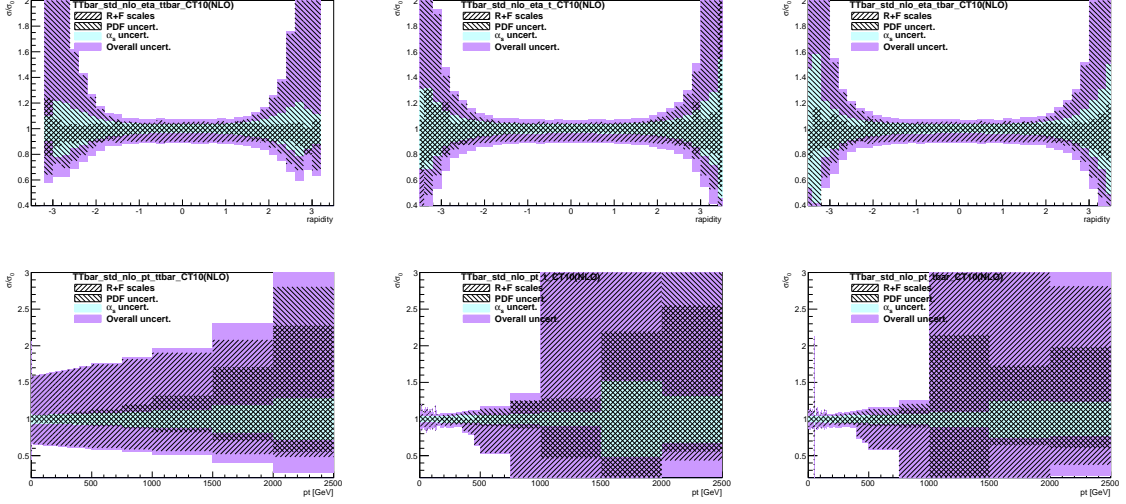


Figure 6: Uncertainties in $t\bar{t}$ production. From left to right the plots are shown for the $t\bar{t}$ pair, t and \bar{t} in the final state. The cross sections σ normalized to the reference cross section without error bands σ_0 are shown with respect to y (first row) and p_T (second row). The jumps in the p_T dissolved plots for the single tops are not physical and due to errors during the event generation.

was done for every PDF listed above. The results are shown in fig.7-9, where now the PDFs are plotted with their overall uncertainties against the 'CT10nlo' reference cross section without errors. That's why the yellow shapes symbolising the cross section uncertainties as predicted by the PDF 'CT10nlo' have exactly the same shape as the purple errorbands depicting the overall uncertainties in fig.4-6. In general it can be seen that the other PDFs qualitatively yield the same cross section uncertainties with narrow error bands in the rapidity dissolved plots for the Z and $b\bar{b}$ productions, the strong increase for larger $|y|$ in the $t\bar{t}$ productions and the increase for large p_T . Also the deviations of the predicted cross sections' means from the reference cross section are usually within the error bands of the respective PDFs, an exception being the rapidity dissolved plots focusing on the lepton/quark pair in the final state (always the first plot in fig.4-6) where the predictions even deviate in the small $|y|$ regime. Looking at the p_T dissolved plots not only the uncertainties of the single PDF cross section predictions became larger, but also their deviations from each other increase. This is again a strong signal that for high p_T the parametrisation of the various PDFs starts to fail, not predicting the right physics anymore.

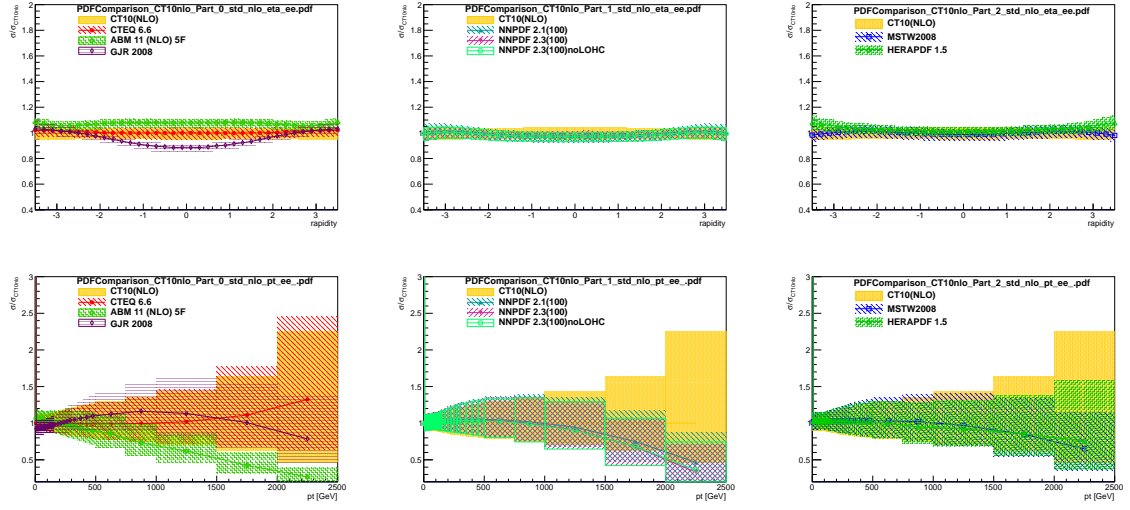


Figure 7: Overall uncertainties in Z production cross sections as predicted by different PDF's. The cross sections σ normalized to the reference cross section of the PDF 'CT10nlo' without error bands σ_0 are shown with respect to y (first row) and p_T (second row).

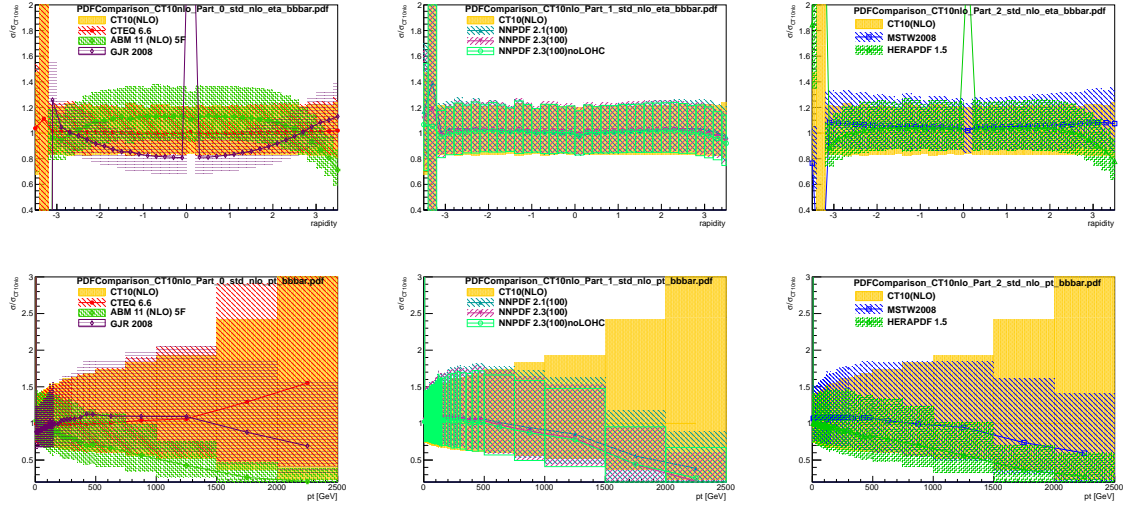


Figure 8: Overall uncertainties in $b\bar{b}$ production cross sections as predicted by different PDF's. The cross sections σ normalized to the reference cross section of the PDF 'CT10nlo' without error bands σ_0 are shown with respect to y (first row) and p_T (second row). The peaks in the first row of plots are not physical and are due to errors during the event generation.

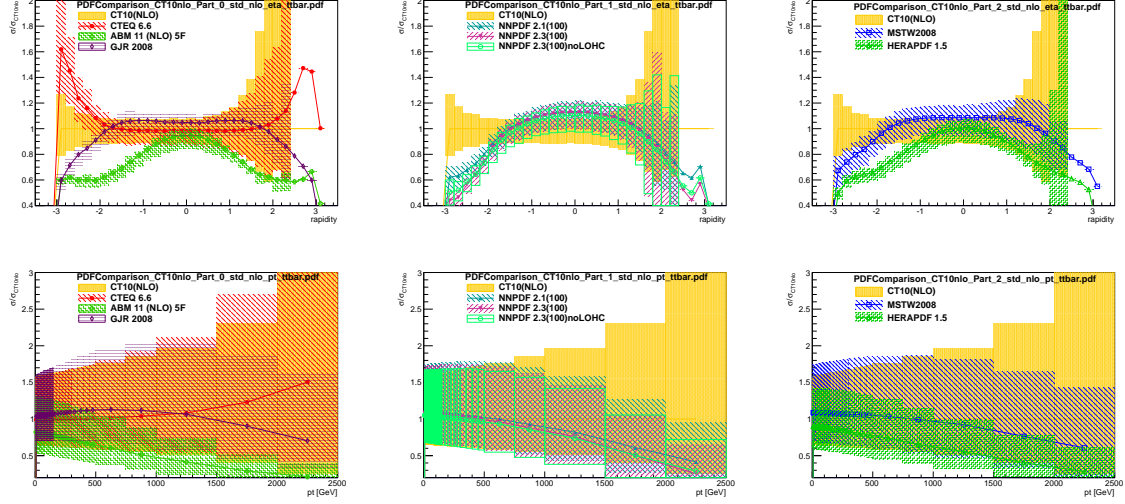


Figure 9: Overall uncertainties in $t\bar{t}$ production cross sections as predicted by different PDF's. The cross sections σ normalized to the reference cross section of the PDF 'CT10nlo' without error bands σ_0 are shown with respect to y (first row) and p_T (second row). The shift of the cross section predicted by 'CT10nlo' to the left is unphysical and due to errors in the analysis.

6 Conclusion

In summary the above analysis showed that for small rapidity $|y| < 2$ and for $p_T < 100$ GeV the various investigated PDFs all predict consistently the same production cross sections with small error bands within the 20% range. In the not yet well measured top production there are strong deviations and high uncertainties in the high rapidity region. The same is true in the high transverse momentum region for all production channels investigated here. This is due to the fact that PDFs are unconstrained in this region.

In the end I want to say that the summer student program 2013 was a great experience for me and want to thank my supervisor P. Starovoitov for the opportunity he gave me by choosing me as his summer student for this year. Under his supervision I was able to improve so many skills especially programming in various computer languages and the use of the analysis tool 'root' and was able to deepen my knowlegde about non-pertubative QCD. Without his experience and help this project report would not have been possible.

References

- [1] J. C. Collins, D. E. Soper and G. F. Sterman, Adv. Ser. Direct. High Energy Phys. **5** (1988) 1 [hep-ph/0409313].
- [2] M. R. Whalley, D. Bourilkov and R. C. Group, hep-ph/0508110.
- [3] G. P. Salam and J. Rojo, Comput. Phys. Commun. **180** (2009) 120 [arXiv:0804.3755 [hep-ph]].
- [4] J. M. Campbell and R. K. Ellis, Phys. Rev. D **62** (2000) 114012 [hep-ph/0006304].
- [5] M. Sutton, T. Carli, D. Clements, A. Cooper-Sarkar, C. Gwenlan, G. P. Salam, F. Siegert and P. Starovoitov, PoS DIS **2010** (2010) 051.